Enzyme structural plasticity and the emergence of broad-spectrum antibiotic resistance.

Frédérique Maurice, Isabelle Broutin, Isabelle Podglajen, Philippe Benas, Ekkehard Collatz, Frédéric Dardel

Enzyme structural plasticity and emergence of broad spectrum antibiotic resistance

Frédérique Maurice[1], Isabelle Broutin[1], Isabelle Podglajen[2], Philippe Benas[1], Ekkehard Collatz[2], Frédéric Dardel[1]

[1]*Cristallographie & RMN Biologiques, Université Paris Descartes, CNRS, 4 avenue de l'Observatoire, 75006, Paris, France.*

[2] *Laboratoire de Recherche Moléculaire sur les Antibiotiques, Université Paris 6, 15 rue de l'Ecole de Médecine, 75006, Paris, France*

Correspondence to Frédéric Dardel
mail: frederic.dardel@univ-paris5.fr
Tel: +33 1 53 73 95 12
Fax: +33 1 53 73 99 25

Running title : Structural basis of emerging antibiotic resistance
Keywords : acetyltransferase, aminoglycoside, antibiotic resistance, ciprofloxacin, crystallography

26115 characters

ABSTRACT

The emergence of multi-resistant pathogenic bacteria is a worldwide health issue. Recently, clinical variants of a single antibiotic-modifying acetyltransferase, AAC(6')-Ib, have appeared that confer extended resistance to most aminoglycosides and, more surprisingly, to structurally unrelated fluoroquinolones. The corresponding gene is carried by mobile genetic elements and is present in most multi-resistant pathogenic strains, hence making it a serious threat to current therapies. We report the crystal structures of both narrow and broad-spectrum resistance variants of this enzyme, which reveal the structural basis for the emergence of extended resistance. The active site displays an important plasticity and has adapted to new substrates by a large-scale gaping process. We have also obtained co-crystals with both substrates, as well as with a simple transition state analog, which provides new clues for the design of inhibitors of this resistance mechanism.

INTRODUCTION

One of the major mechanisms of antibiotic resistance is the enzymatic modification of the active compound which prevents its binding to the cellular target. Aminoglycosides and fluoroquinolones are potent, broad-spectrum antibiotics of major clinical importance. Until recently, they escaped this resistance mechanism to different degrees, which preserved them as key drugs for treating life-threatening infections caused by resistant bacteria. While no enzymatic modification of the synthetic fluoroquinolones had been observed, the known aminoglycoside-modifying enzymes with their somewhat limited substrate specificities could not simultaneously inactivate all clinically used compounds. One of the most common mechanisms is *N*-acetylation at the 6' position (Vakulenko & Mobashery, 2003) (Fig 1A), catalyzed by the aminoglycoside 6'-*N*-acetyltransferases (AAC(6')). Two functional classes of this enzyme have been described: AAC(6')-I, conferring resistance to amikacin but not to gentamicin, and AAC(6')-II, with the reciprocal selectivity (both classes also acetylate kanamycin, tobramycin, neomycin, netilmicin and sisomicin). Now, isoforms of the AAC(6')-Ib subclass have evolved in clinical isolates with the capacity to modify amikacin as well as gentamicin or some fluoroquinolones.

This has a strong clinical relevance, as AAC(6')-Ib is the most prevalent aminoglycoside-modifying enzyme, present in over 70% of AAC(6')-producing gram-negative isolates (Vakulenko & Mobashery, 2003). Its spread may have been favored by integration of its gene into natural expression vectors such as integrons (Fluit & Schmitz, 2004). Among the recent variants of this enzyme with altered specificity are AAC(6')-Ib_{11} which confers simultaneous resistance to gentamicin and amikacin (Casin *et al*, 2003) and AAC(6')-Ib-cr, which has a unique extension of its substrate specificity from aminoglycosides to structurally unrelated fluoroquinolones (Robicsek *et al*, 2006b). Both variants differ from the initially identified AAC(6')-Ib (Tran Van Nhieu & Collatz, 1987) (aside from functionally irrelevant *N*-terminal differences) by two amino acid substitutions each and are currently spreading (Robicsek *et al*, 2006a) (supplementary Fig 1 online).

Two structures of AAC(6')-I have been reported, AAC(6')-Ii and AAC(6')-Iy (Wybenga-Groot *et al*, 1999; Vetting *et al*, 2004). These two enzymes are chromosomally-encoded and hence confined to a single bacterial species. They confer a low level of resistance and their primary function as aminoglycoside resistance enzymes has been questioned (Magnet *et al*, 2001). Accordingly, they have moderate catalytic efficiencies and/or affinities for aminoglycosides, about one to two orders of magnitude lower than those of AAC(6')-Ib (Kim

et al, 2007; Magnet *et al*, 2001; Wright & Ladak, 1997). Their sequences are also quite divergent from that of the predominant AAC(6')-Ib (identity level < 20%, supplementary Fig 1 online), therefore, they cannot be used to provide structural insights into the broadenings of AAC(6')-Ib specificity and its current clinical consequences.

In the present work, we report the structure of narrow and broad-spectrum variants of AAC(6')-Ib, free and complexed. Interaction with the antibiotic substrate is different from that of AAC(6')-Iy and allows both tighter binding and broader recognition of second-generation aminoglycosides, such as amikacin. Furthermore, we show that the mutations which are responsible for spectrum broadening induce a large structural change in the active site, which allows for the accommodation of an extended set of substrates.

RESULTS AND DISCUSSION

We have solved the crystal structures of both AAC(6')-Ib and AAC(6')-Ib_{11}. The narrow spectrum variant Ib was crystallized in complex with coenzyme A (structure solved to 1.8 Å resolution), or coenzyme A and kanamycin (2.4 Å resolution). Crystals of broad-spectrum variant Ib_{11} were obtained the absence of substrate (2.1 Å resolution). Interestingly, each variant failed to crystallize in the conditions used for the other one. Both variants share the same fold (Fig 1B), which belongs to the GCN5-related *N*-acetyltransferase superfamily (Vetting *et al*, 2005), also encompassing other classes of AAC. Accordingly, the acetyl-CoA binding site is structurally similar to that of other enzymes of this family. Even if the cofactor was not co-crystallized with the AAC(6')-Ib_{11}, the corresponding binding pocket is similar to that of AAC(6')-Ib (supplementary Fig 2 online). There are, however, important differences at the level of the antibiotic binding site, which will be discussed below.

The two previously reported AAC(6') structures are dimers and their aminoglycoside binding crevice is shared between the two protomers (Vetting *et al*, 2004; Wybenga-Groot *et al*, 1999) (supplementary Fig 3 online). On the contrary, AAC(6')-Ib is essentially monomeric: gel filtration experiments confirmed that AAC(6')-Ib and AAC(6')-Ib-cr are monomers in solution, whereas AAC(6')-Ib_{11} exhibits a monomer/dimer equilibrium (not shown). Accordingly, the active site is contained within a single protomer, with the aminoglycoside binding site being constituted by connecting loops (Fig 1B), a topology that differs from the previously reported structures. These loops form a closed pocket, in which the aminoglycoside fits snugly (Fig 2A).

There is also a long α-helical flap forming a lid over the antibiotic pocket, with a loop contacting the aminoglycoside rings (Fig 1B). This extended flap is specific of ACC(6')-Ib (supplementary Figs 1 and 3 online) and is held in place by a stacking interaction between the side chains of W38 (in the flap) and N147 (in the core, Fig 2B), creating a tunnel surrounding the end of the pantetheine arm of coenzyme A. This could explain the specific enzymatic behavior of AAC(6')-Ib, which exhibits an ordered kinetic mechanism, in which acetyl-CoA is the first substrate to bind (Kim *et al*, 2007). Locking of the flap around acetyl-CoA could therefore position key residues involved in antibiotic recognition, such as W39, which stacks onto the aminoglycoside ring I. Hence, prior binding of acetyl-CoA could facilitate subsequent recognition of the antibiotic.

AAC(6')-Ib has evolved the capacity to acetylate semi-synthetic aminoglycosides that carry a bulky *N*-substituent on the central ring, such as amikacin (Fig 1A). There indeed exists a cavity on the surface of the active site that can accommodate such a chain (Fig 2A). This binding pocket is absent in the active site of other, less efficient variants of AAC(6').

Mutations which confer a broadened spectrum to AAC(6')-Ib$_{11}$, Q106L and L107S (purple in Fig 1C), are not located in the immediate vicinity of the aminoglycoside site, but along the narrow groove that binds the pantetheine arm of acetyl-CoA. In AAC(6')-Ib$_{11}$, the double substitution induces a large structural change, caused by a disruption of the central β-strand (Fig 1C and supplementary figure 4 online). As a consequence, the packing of helices above and below the β-sheet is perturbed, causing a large scale "gaping" of the active site, with W38 moving by as much as 15 Å. Several lines of evidence indicate that this structural change is genuine, and not a consequence of crystal packing. It is direct structural effect: in the wild-type structure, the side chain of W39, in the flap, interdigitates between residues 105 and 107, an interaction obstructed by the double mutation at this site (supplementary Fig 4 online). This structural change involving W38 and W39 also induces a redshift of the intrinsic fluorescence of the mutant protein in solution, suggesting that they are indeed more exposed to the solvent in the latter structure (supplementary Table 1 online). It is thus likely that the flap will be quite flexible in the AAC(6')-Ib$_{11}$ mutant with several possible conformations among which that observed in the crystals could be trapped by packing. This structural changes result in a major increase in the accessible volume of the active site which could then possibly accommodate bulkier substrates with substituted amino groups. In addition, the carboxylate group of D105, next to the double mutation, could also contribute directly to render the secondary *N*6' amine of gentamicin more acidic and hence more reactive to acetylation (supplementary Fig 5 online). This might explain the dual specificity of this variant for gentamicin and amikacin.

AAC(6')-Ib$_{11}$, which was crystallized in the absence of substrate, serendipitously co-crystallized with one HEPES buffer molecule bound within the active site (Fig 3B). Remarkably, the sulfonate group of HEPES lies over the position of the sulfur atom of coenzyme A and the nitrogen atom of its piperazine ring sits at the site of the acetylatable nitrogen of kanamycin. Using solution NMR, we observed direct saturation transfer from the protons of the enzyme to those of HEPES, confirming that HEPES is able to bind to AAC(6'), not only in crystals, but also in solution (supplementary Fig 6 online). Hence HEPES appears

as a minimal transition state analog of the acetylation reaction (Fig 3A) and could thus be used as a central scaffold for building effective inhibitors of AAC(6') enzymes.

Interestingly, one of the fluoroquinolones which AAC(6')-Ib-cr has evolved to recognize, ciprofloxacin, also contains a piperazine moiety (Fig 3A) which is *N*-acetylated by the enzyme (Robicsek *et al*, 2006b). The two substitutions which confer the new specificity to AAC(6')-Ib-cr, W92R and D169Y, are located in two exposed loops which form the backside of the antibiotic binding pocket (Fig 1B). It appeared therefore straightforward to model the structure of AAC(6')-Ib-cr based on that of AAC(6')-Ib. The interaction with ciprofloxacin was investigated, using the structural similarity with HEPES to anchor the piperazine ring of the fluoroquinolones in the enzyme. The result of this modeling (Fig 3C) shows the side-chains of the two substituted residues being in a position to form specific stabilizing interactions with ciprofloxacin: Y169 can stack on the quinolone heterocycle, while the guanidinium group of R92 can hydrogen bond to the keto or carboxy groups of the antibiotic.

In addition to the "gaping" capability of the active site, the specific scaffold of AAC(6')-Ib, in which recognition of the acetylatable substrate is mediated by side-chains of exposed loops (as opposed to other AAC(6') enzymes), could provide the structural plasticity required for adaptation to new antibiotics. This could explain in part why this isoform has been selected under the pressure of antibiotic usage and is now widely distributed among pathogens. Conversely, such a broad distribution makes AAC(6')-Ib an attractive target for countering drug resistance. The reported structures could help in guiding the design of novel aminoglycosides circumventing resistance. In addition, the observation that an original scaffold (piperazine ethane sulfonate) can mimic the transition sate, could be an interesting lead for designing novel inhibitors.

METHODS

Plasmid construction and protein expression

AAC(6')-b_{11} was originally identified in *Salmonella enterica* (Casin *et al*, 2003). Its sequence was PCR amplified and cloned in pET101 (Invitrogen) and expressed in *E. coli* (Maurice *et al*, 2006). This protein showed a significant propensity to aggregate and was expressed in inclusion bodies at growth temperatures above 20°C. We used a phenotypic screen to select for increased solubility. Transformed *E. coli* cells were streaked on LB plates containing kanamycin (50μg/ml) and incubated at 37°C. Cells expressing soluble AAC(6')-Ib were able to grow normally as they could acetylate the antibiotic, whereas those expressing insoluble forms were selected against. After DNA sequencing, one such resistant variant was shown to carry a single nucleotide deletion in the stop codon. This results in a C-terminal extension of the protein by a hydrophilic tail of seven aminoacids, EGRAQFE (supplementary Fig 1 online). This "tagged" variant proved to be stable and soluble. It was kept for further studies, as it is otherwise identical to the original AAC(6')-b_{11} and shows a similar antibiotic selectivity. Purification of this protein was achieved as described (Maurice *et al*, 2006). Expression vectors for wild type AAC(6')-Ib and variant AAC(6')-Ib-cr were derived by site-directed mutagenesis of the AAC(6')-Ib_{11} vector (QuikChange, Stratagene) and the corresponding proteins also contain the solubility tag. The function of these various AAC(6')-Ib was monitored by *in vivo* functional resistance assays (supplementary Table 2 online).

Protein crystallization

Crystals of AAC(6')-Ib were grown at 18°C by the hanging-drop method from a solution containing 1.5M K_2HPO_4, 0.06M NaH_2PO_4, 0.1M guanidine-HCl and were reproduced by streak seeding. Crystals were stabilized in 15% glycerol, 1.6 M K_2HPO_4, 0.07 M NaH_2PO_4 before vitrification in liquid N_2. Crystals belong to space group $P4_32_12$ with unit cell constants of $a = b = 57.62$ Å and $c = 146.67$ Å.

Crystals of AAC(6')-Ib_{11} and Se-Met-AAC(6')-Ib_{11} were grown at 18 °C by the hanging–drop method by mixing equal volumes of protein (15 mg/ml) and reservoir solution (100 mM HEPES pH 7.5, 1.5 M Li_2SO_4, 3% isopropanol). Crystals belong to space group $C222_1$ with unit cell constant of $a = 71.62$ Å, $b = 85.37$ Å, and $c = 150.41$ Å.

Structure determination and refinement

A multiwavelength anomalous diffraction data set was collected on a Se-Met AAC(6')-Ib_{11} crystal to 2.8 Å resolution on the BM30A beam line (ESRF, Grenoble). Datasets were

collected at λ=0.9794 Å (inflexion), λ=0.9792 Å (peak) and λ=0.9278 Å (remote). They were integrated and scaled with XDS (Kabsch, 1993). Model building was done with Sharp and O (Jones *et al*, 1991). A 2.1 Å resolution native dataset of AAC(6')-Ib_{11} was also collected on ID14 (ESRF, Grenoble), the refinement was performed in CNS (Brunger *et al*, 1998) (crystallographic parameters in supplementary Table 3 online).

The structure of AAC(6')-Ib was solved with Phaser (Read, 2001) using the AAC(6')-Ib_{11} as a molecular replacement model. The model was completed using iterative cycles of model building and refinement in REFMAC (Winn *et al*, 2001). Although not added in the crystallization solution, electron density due to bound CoA was observed, a situation previously reported for AAC(6')-Iy (Vetting *et al*, 2004). The structure of the complex with kanamycin was obtained by diffusing the antibiotic into the crystals (1 to 1 ratio with the protein) and solving the structure similarly. 2 F_o-F_c density maps of the CoA and kanamycin are shown in supplementary Fig 7 online.

Completeness of the models was 173 out of 196 residues for both the AAC(6')-Ib and AAC(6')-Ib_{11} structures. Density was missing for residues 1-10 and 184-196 in AAC(6')-Ib_{11} and 1-11, 41-43 and188-196 in AAC(6')-Ib. The missing N- and C-terminal extensions are not part of the enzyme core. The C-terminal extension corresponds to the solubility tag, whereas the N-terminal extension originates from gene fusion (Casin *et al*, 1998).

AAC(6')-Ib_{11} crystals contain two monomers per asymmetric unit whereas the wild-type enzyme contains only one and is a true monomer in solution (not shown). The former observation could be related to the fact that AAC(6')-Ib_{11} variant appears to be partially dimeric in gel filtration experiments (not shown). The protein-protein contact seen in the crystal structure of this protein differ from those observed in the structure of other AAC(6').

Coordinates have been deposited with the PDB (entries 2PRB, 2QIR and 2PR8).

Saturation transfer difference.

NMR setup and saturation transfer difference experiments (Mayer & Meyer, 2001) using AAC(6')-Ib11 were performed as previously described (Maurice *et al*, 2006; Tisne & Dardel, 2002).

Modeling the interaction with ciprofloxacin

Starting from the structure of wild-type AAC(6')-Ib, the two mutations (W92R and D169Y, suppl. Fig 1) were introduced manually using Pymol (DeLano Scientific). The corresponding structure was energy minimized using X-PLOR-NIH (Schwieters *et al*, 2003). Ciprofloxacin

structure was generated using PRODRG (Schuttelkopf & van Aalten, 2004). Six different rotamers of ciprofloxacin were generated, by rotation about the piperazine-quinolone bond. They were then placed into the active site of AAC(6')-Ib-cr, by superimposing their piperazine ring onto that of HEPES in the structure of AAC(6')-Ib_{11}, ignoring steric clashes. These six complexes were refined independently. Cα atoms of residues outside the active site (residues 12-38, 44-87, 95-163 and 174-187) were restrained by a harmonic potential, as well as the acetylatable nitrogen of ciprofloxacin, in order to maintain the active site geometry. The complex was energy minimized and submitted to a restrained simulated annealing refinement. It consisted of 2 ps of dynamics at 1000 K followed by cooling to 100 K over 10 ps during which the harmonic restraints on the Cα atoms were gradually turned off. The resulting complexes were finally energy minimized.

Of the six resulting structures, two had poor energy scores and were discarded. The other four were very similar, with both rings of ciprofloxacin in comparable orientations. In some structures, the mutated residues (R92 and Y169) had come in contact with the ligand, suggesting they contributed directly to binding. In order to model these interactions, we submitted the four structures to an additional short restrained molecular dynamics refinement (5 ps at 100K followed by minimization). We added distance restraints, forcing the guanidinium of R92 and the ring of Y169 to contact ciprofloxacin. This resulted in structures in which R92 contacted the oxo or carboxy oxygen of ciprofloxacin, while Y169 stacked on top of the quinolone. All four structures were similar and had good stereochemistry. The best structure is shown in Fig 3C.

ACKNOWLEDGMENTS

The authors gratefully acknowledge Drs. Claudine Mayer and Sabrina Biarrotte-Sorin for initial advice on structure determination. FM is supported by a scholarship from the French Ministry of research and higher education.

REFERENCES

Brooks BR, Bruccoleri RE, Olafson BD, States DJ, Swaminathan S, Karplus M (1983) Charmm - a Program for Macromolecular Energy, Minimization, and Dynamics Calculations. *J Comp Chem* **4**: 187-217

Brunger AT, Adams PD, Clore GM, DeLano WL, Gros P, Grosse-Kunstleve RW, Jiang JS, Kuszewski J, Nilges M, Pannu NS, Read RJ, Rice LM, Simonson T, Warren GL (1998) Crystallography & NMR system: A new software suite for macromolecular structure determination. *Acta Crystallogr D Biol Crystallogr* **54**: 905-921

Casin I, Bordon F, Bertin P, Coutrot A, Podglajen I, Brasseur R, Collatz E (1998) Aminoglycoside 6'-N-acetyltransferase variants of the Ib type with altered substrate profile in clinical isolates of Enterobacter cloacae and Citrobacter freundii. *Antimicrob Agents Chemother* **42**: 209-215

Casin I, Hanau-Bercot B, Podglajen I, Vahaboglu H, Collatz E (2003) Salmonella enterica serovar Typhimurium bla(PER-1)-carrying plasmid pSTI1 encodes an extended-spectrum aminoglycoside 6'-N-acetyltransferase of type Ib. *Antimicrob Agents Chemother* **47**: 697-703

Fluit AC, Schmitz FJ (2004) Resistance integrons and super-integrons. *Clin Microbiol Infect* **10**: 272-288

Jones TA, Zou JY, Cowan SW, Kjeldgaard M (1991) Improved methods for building protein models in electron density maps and the location of errors in these models. *Acta Crystallogr A* **47**: 110-119

Kabsch W (1993) Automatic Processing of Rotation Diffraction Data from Crystals of Initially Unknown Symmetry and Cell Constants. *J Appl Cryst* **26**: 795-800

Kim C, Villegas-Estrada A, Hesek D, Mobashery S (2007) Mechanistic Characterization of the Bifunctional Aminoglycoside-ModifyingEnzyme AAC(3)-Ib/AAC(6')-Ib' from *Pseudomonas aeruginosa*. *Biochemistry* **46**: 5270-5282

Magnet S, Lambert T, Courvalin P, Blanchard JS (2001) Kinetic and Mutagenic Characterization of the Chromosomally Encoded *Salmonella enterica* AAC(6')-Iy Aminoglycoside N-Acetyltransferase. *Biochemistry* **40**: 3700-3709

Maurice F, Bégis B, Micouin L, Dardel F (2006) NMR Identification of ligands of aminoglycoside resistance enzymes. *C R Chimie* **9**: 413-419

Mayer M, Meyer B (2001) Group epitope mapping by saturation transfer difference NMR to identify segments of a ligand in direct contact with a protein receptor. *J Am Chem Soc* **123**: 6108-6117

Read RJ (2001) Pushing the boundaries of molecular replacement with maximum likelihood. *Acta Crystallogr D Biol Crystallogr* **57**: 1373-1382

Robicsek A, Jacoby GA, Hooper DC (2006a) The worldwide emergence of plasmid-mediated quinolone resistance. *Lancet Infect Dis* **6**: 629-640

Robicsek A, Strahilevitz J, Jacoby GA, Macielag M, Abbanat D, Park CH, Bush K, Hooper DC (2006b) Fluoroquinolone-modifying enzyme: a new adaptation of a common aminoglycoside acetyltransferase. *Nat Med* **12**: 83-88

Schuttelkopf AW, van Aalten DM (2004) PRODRG: a tool for high-throughput crystallography of protein-ligand complexes. *Acta Crystallogr D Biol Crystallogr* **60**: 1355-1363

Schwieters CD, Kuszewski JJ, Tjandra N, Clore GM (2003) The Xplor-NIH NMR molecular structure determination package. *J Magn Reson* **160**: 65-73

Tisne C, Dardel F (2002) Optimisation of a Peptide library for screening specific RNA ligands by flow-injection NMR. *Comb Chem High Throughput Screen* **5**: 523-529.

Tran Van Nhieu G, Collatz E (1987) Primary structure of an aminoglycoside 6'-N-acetyltransferase AAC(6')-4, fused in vivo with the signal peptide of the Tn3-encoded beta-lactamase. *J Bacteriol* **169**: 5708-5714

Vakulenko SB, Mobashery S (2003) Versatility of aminoglycosides and prospects for their future. *Clin Microbiol Rev* **16**: 430-450

Vetting MW, LP SdC, Yu M, Hegde SS, Magnet S, Roderick SL, Blanchard JS (2005) Structure and functions of the GNAT superfamily of acetyltransferases. *Arch Biochem Biophys* **433**: 212-226

Vetting MW, Magnet S, Nieves E, Roderick SL, Blanchard JS (2004) A bacterial acetyltransferase capable of regioselective N-acetylation of antibiotics and histones. *Chem Biol* **11**: 565-573

Winn MD, Isupov MN, Murshudov GN (2001) Use of TLS parameters to model anisotropic displacements in macromolecular refinement. *Acta Crystallogr D Biol Crystallogr* **57**: 122-133

Wright GD, Ladak P (1997) Overexpression and Characterization of the Chromosomal Aminoglycoside 6'-N-Acetyltransferase from *Enterococcus faecium*. *Antimicrob Agents Chemother* **41**: 956-960

Wybenga-Groot LE, Draker K, Wright GD, Berghuis AM (1999) Crystal structure of an aminoglycoside 6'-N-acetyltransferase: defining the GCN5-related N-acetyltransferase superfamily fold. *Structure* **7**: 497-507

FIGURE LEGENDS

Figure 1. Structure of AAC(6')-Ib and structural switch associated with broad-spectrum inducing substitutions. (A) Structure of gentamicin and amikacin. The amino groups which are acetylated are indicated by arrows. (B) Topology of AAC(6')-Ib. Residue numbers are indicated. The yellow disk indicates the location of the aminoglycoside binding pocket. The top of this pocket is closed by an alpha helical flap which folds back along the dashed axis, above the central β-sheet. (C) Structure of AAC(6')-Ib (left) and of its broad-spectrum variant AAC(6')-Ib_{11} (right). Substituted residues are shown in purple. Pink arrows indicate movements of the flap and W38. Color coding is the same for panels B and C.

Figure 2. Recognition of ligands. (A) structure of AAC(6')-Ib in complex with kanamycin. The solvent accessible surface is shown, colored as a function of the electrostatic surface potential. The oval contour highlight the crevice that could accommodate N3 substituents of 2-DOS, such as that present in amikacin. (B) Locking of the "flap" around coenzyme A. N146 is hydrogen bonded to the pantetheine arm and provides a stacking platform for the side chain of W38 in the flap. This contributes to position W39 which is part of the antibiotic binding pocket.

Figure 3. Interaction of AAC(6')-Ib with ligands. (A) Comparison of ligand geometries : top acetyl-CoA and aminoglycoside; middle, HEPES; bottom, acetyl-CoA and ciprofloxacin. (B) 2 Fo-Fc electron density of HEPES bound in the active site of AAC(6')-Ib_{11} contoured at 2σ. (C) refined model of ciprofloxacin bound to AAC(6')-Ib-cr, showing interactions with the two mutated residues, R92 and Y169 (same color coding as in Fig 1).

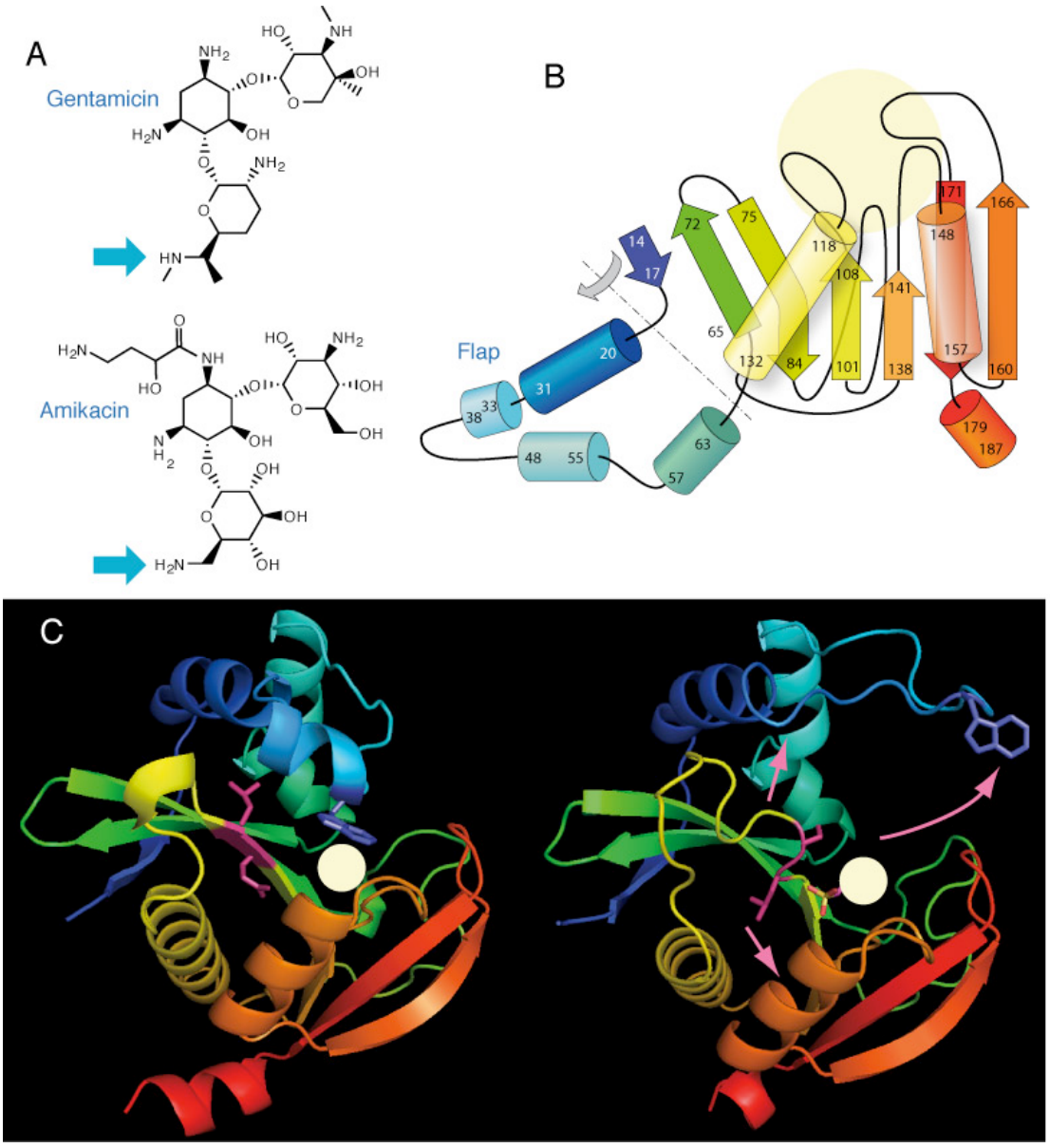
A
Gentamicin
Amikacin
B
Flap
14
17
72
75
118
108
65
132
84
101
141
138
148
171
166
157
160
20
31
33
38
48
55
63
57
179
187
C

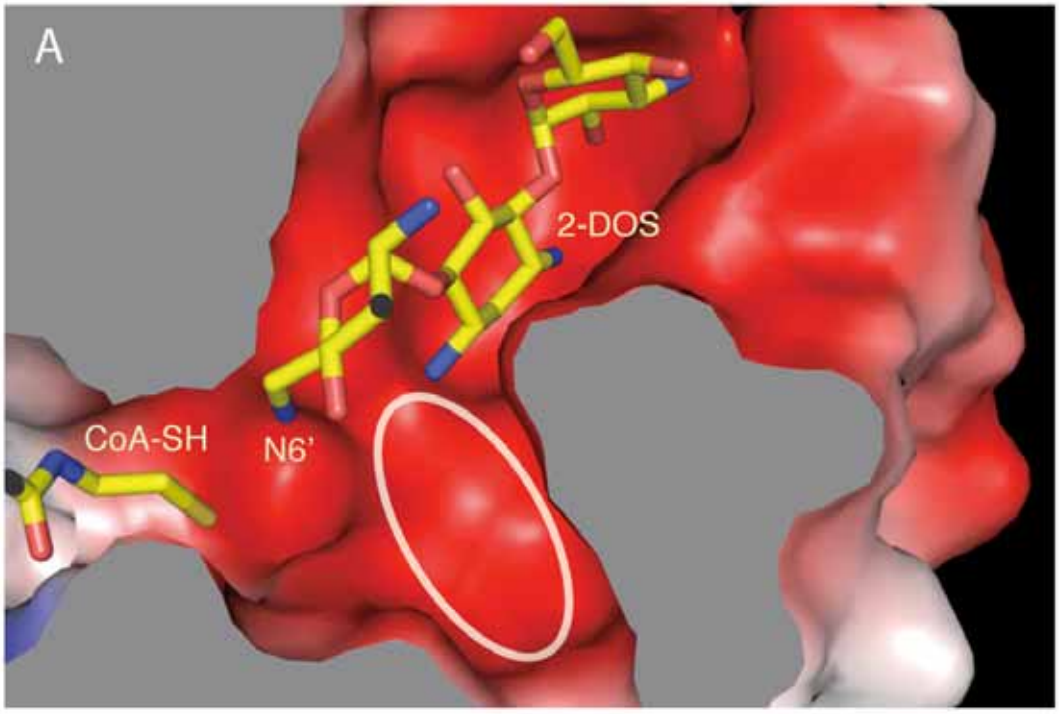
A
2-DOS
CoA-SH
N6'

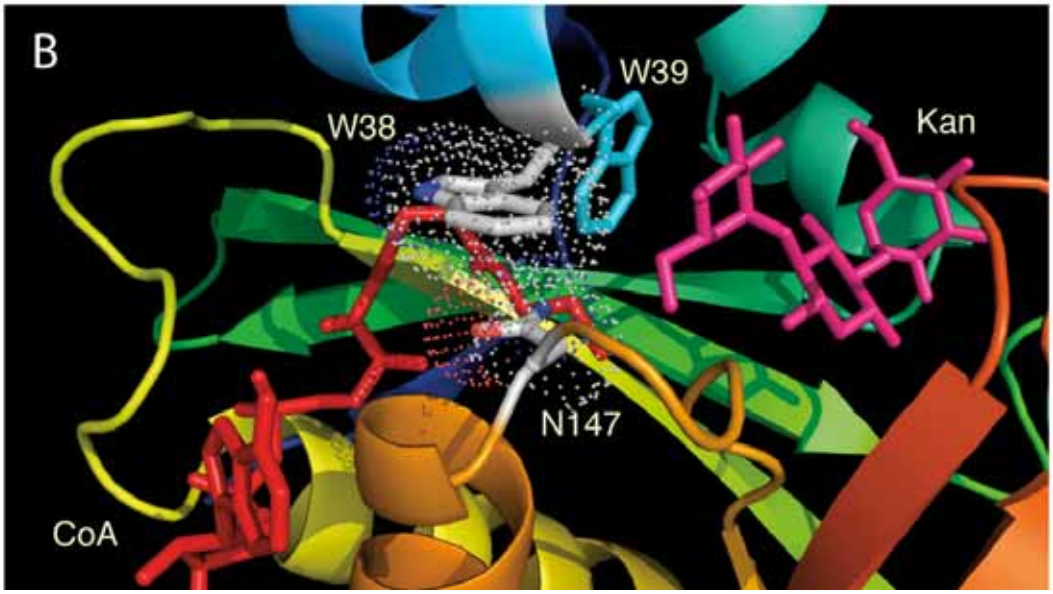
B
W39
W38
Kan
N147
CoA

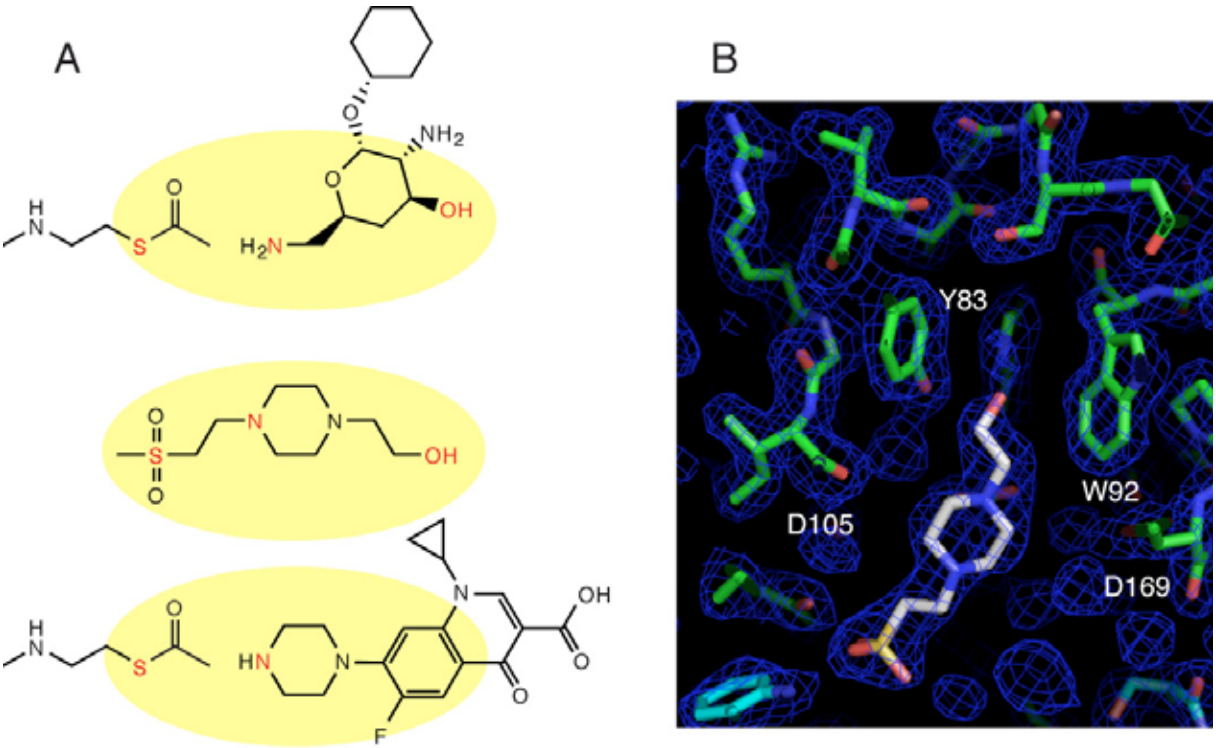
A
B
Y83
W92
D105
D169
C
Y169
R92
D105
W93